

RIP
THE MACHO ERA (1974-2004)

N.W. EVANS, V. BELOKUROV
Institute of Astronomy, Madingley Rd
Cambridge CB3 0HA, England
E-mail: nwe@ast.cam.ac.uk, vasily@ast.cam.ac.uk

This article reviews the life and death of a scientific theory

1. The MACHO Ideology

1.1. *The Dawn of Dark Matter*

The hypothesis of dark matter is often ascribed to Fritz Zwicky. Certainly, Zwicky ¹ in his book “Morphological Astronomy” noted the discrepancy between masses of clusters inferred from the virial theorem and masses inferred from the visible constituent galaxies. He suggests five possible explanations. The fifth (and most tentative) — after propositions that the clusters may not be in equilibrium or that light may tire on traversal of enormous distances — is: “*Finally, attention must be called to the recent discovery of luminous and of dark intergalactic matter. The existence of this dark matter may seriously affect all previous estimates concerning the distribution of mass in the Universe*”.

The focus of this conference is on the direct and indirect detection of dark matter in the Milky Way galaxy and other nearby galaxies. Even if Zwicky was the first to hypothesise the existence of dark matter in clusters, he did not believe that there was appreciable dark matter in galaxies (in “Morphological Astronomy”, he advocated Keplerian fitting to rotation curves to estimate the masses of galaxies). The realisation that galaxies are surrounded by dark matter haloes only came much later. Dark matter on the scales of galaxies became widely accepted after the publication of the rotation curve of the nearby galaxies M31, M81 and M101 by Roberts and collaborators ². In an influential paper, Ostriker, Peebles & Yahil ³ brought together a number of lines of evidence to suggest that: “*There*

are reasons, increasing in number and in quality, to believe that the masses of ordinary galaxies may have been underestimated by a factor of 10 or more. . . The very large implied mass to light ratios and very great extent of spiral galaxies can perhaps most plausibly be understood as due to a giant halo of faint stars”

This is the first statement of the MACHO ideology – namely that (some of) the dark matter in galaxy haloes is baryonic and composed of massive objects. The most obvious candidates are faint stars (red dwarfs, white dwarfs, neutron stars), failed stars (brown dwarfs and Jupiters) and massive remnants from an early epoch of Population III stars. The neologism MACHO seems to have been first used in print by Griest ⁴ as a witty counterpoise to WIMPS (weakly interacting massive particles). MACHO stands for massive compact halo objects.

1.2. *The Hey-Day of the MACHO Era (1974-1994)*

The Zeitgeist is well documented in the Princeton conference on “Dark Matter in the Universe”, which marks the hey-day of the MACHO Era. It was well-known that all the dark matter in galaxies and clusters could conceivably be baryonic without violating constraints from cosmological nucleosynthesis ⁵. There even seemed to be arguments in favour of baryonic compact objects as opposed to particle dark matter. For example, Gunn ⁶ pointed out that; *“There is evidence that the Population II mass function is very steep in the halo and an extension at the low mass-end to quite plausible masses leads to very large mass-to-light ratios. . . A picture in which the low-mass cut-off progresses smoothly from $0.1 M_{\odot}$ to $10^{-3} M_{\odot}$ as one goes from the center of the galaxy outwards makes a qualitatively plausible model. . . It entails no mystery as to why the amount of dark matter is within an order of magnitude of the visible matter, and makes plausible the fact that rotation curves are flattish from regions where the galaxies are dominated by visible matter out to regions in which they are dominated by dark matter.”*

More exuberantly still, Lynden-Bell ⁷ cited the X-ray data; *“We have rather good evidence that around a number of giant elliptical galaxies, baryonic matter is disappearing from hot, X-ray emitting gas. The place where it disappears is right for the making of dark halos. The rate of its disappearance would build a halo in 10^{10} years. If we want to believe the observations rather than our prejudices, we should take as our best bet that dark halos are baryonic and made from cooling flows. . . When exotic neutral particles have been found in the laboratory, I shall be happy to postulate them in the*

cosmos, but until then, let us use our observations, not our prejudices.”

But even then, the most important objection to baryonic dark matter as the dominant component of galaxy haloes was clearly understood. It is difficult to understand how such baryonic structures of mass $\sim 10^{12}M_{\odot}$ could have formed without leaving an imprint in the microwave background ⁶.

1.3. *The Decline and Fall of the MACHO Era (1994-2004)*

Microensing as a test for dark, compact objects was suggested very early on (e.g., Zwicky’s “Morphological Astronomy” discusses microensing by neutron stars). But, Paczyński ⁸ convinced the astronomical community that microensing could provide a decisive test of the MACHO hypothesis. And so it turned out The microensing experiments led to the decline and fall of the MACHO Era.

Beginning in 1993, large scale monitoring of stars in the Large Magellanic Cloud (LMC) was conducted by two groups (MACHO and EROS) looking for microensing events. The results of the MACHO experiment are well-known. From 5.7 years of data, Alcock et al. ⁹ found between 13 to 17 microensing events and reckoned that the microensing optical depth (or probability of microensing) is $\tau \sim 1.2_{-0.3}^{+0.4} \times 10^{-7}$. Interpreted as a dark halo population, the most likely fraction of the dark halo in MACHOs is 20 %, while the most likely mass of the MACHOs is between 0.15 and 0.9 M_{\odot} . After 8 years of monitoring the Magellanic Clouds, the EROS experiment announced 3 microensing candidates towards the LMC ¹⁰. Although EROS do not report their results in terms of optical depth, they have clearly detected a smaller microensing signal than MACHO – a discrepancy which could have a number of explanations.

The remainder of this article will argue that Alcock et al. overestimated the microensing optical depth and that the dark halo has little or no MACHOs.

2. Neural Network Processing

There are two principal difficulties with the microensing experiments. The first is well-known, the second less so (and thus we concentrate upon it here).

First, just as in direct detection experiments for particle dark matter, there is a background that must be eliminated. In microensing experiments, stars in the thin disk, thick disk and the LMC all provide possible lenses for microensing events ¹¹, aside from MACHOs in the dark halo.

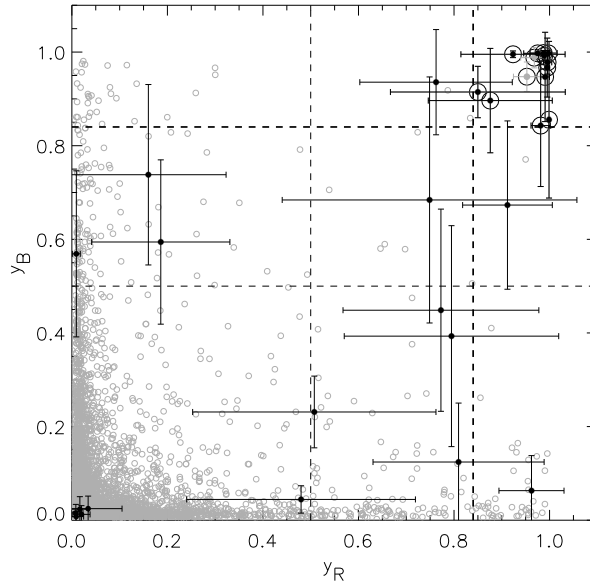


Figure 1. The locations of ≈ 22000 lightcurves as given by the outputs of the neural networks y_R and y_B on processing the red data and the blue data respectively. These include the 29 lightcurves that passed the loose selection of the MACHO collaboration together with ~ 1000 lightcurves in the vicinity of each candidate. Each point gives the maximum of the moderated output while the error bar gives the network scatter. A large open circles around a point indicates that it lies above the decision boundary ($y_R > 0.87$ and $y_B > 0.87$). Filled black dots represent the 29 lightcurves selected by Alcock et al., while all other lightcurves are represented by open grey dots. [From Belokurov et al. 2004]

The total optical depth due to stellar lensing from known populations¹² is $\sim 0.7 \times 10^{-7}$, which is within the 2σ lower bound of Alcock et al.'s claimed detection ($\tau \sim 1.2_{-0.3}^{+0.4} \times 10^{-7}$).

Secondly, the identification of microlensing events (stars that brighten and then fade) takes place against a background of stellar variability that is at least 10^5 times more common. Many varieties of stellar variability are not well-studied or understood. Therefore, the identification of events is much more fraught than usually appreciated. All microlensing groups use a sequence of straight line cuts to identify events (for example, excising chromatic lightcurves or troublesome regions of the colour-magnitude diagram). The decision boundary between microlensing and non-microlensing is therefore polygonal in a multi-dimensional parameter space. Nowadays,

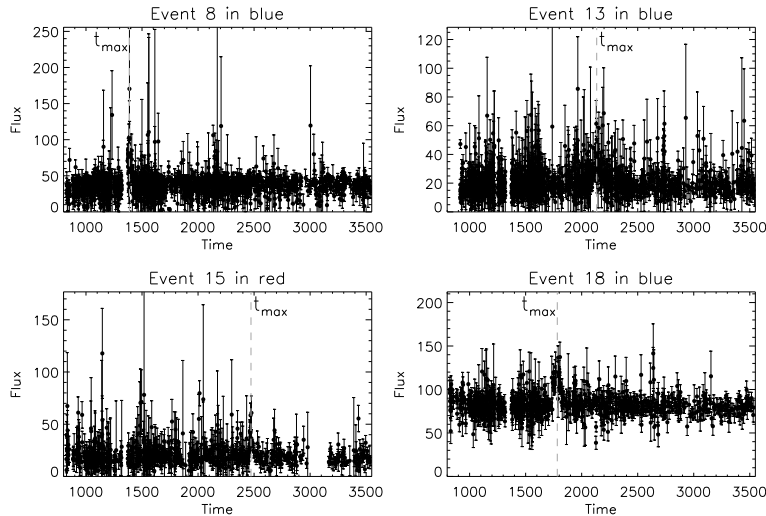


Figure 2. This shows the lightcurves for 4 events which received low probability values y in one or both filters. These are all included in Alcock et al.'s (2000) set of convincing microlensing candidates, but are not confirmed by our neural network analysis. The vertical axis is flux in ADU s^{-1} and the horizontal axis is time in $\text{JD}-2448000$. Vertical lines mark the peak of the event. [From Belokurov et al. 2004]

many high-energy physics experiments prefer to use neural networks for pattern recognition. This is because neural networks permit the construction of complicated decision boundaries.

All this inspired Belokurov, Evans & Le Du¹³ to carry out a re-analysis of the MACHO data with neural networks. Microlensing events are characterised by the presence of (i) an excursion from the baseline that is (ii) positive, (iii) symmetric and (iv) single. The event itself is parameterised by (v) a timescale. Motivated by these features, five parameters are extracted from the lightcurves as inputs to the neural networks. Most neural networks require a training set, on which the network is taught to recognise the desired patterns (in this case, microlensing). Here, the training set contains 1500 examples of microlensing and > 2000 examples of other kinds of variability (pre-main sequence stars, Coronae Borealis stars, Miras, Semi-regular variables, Cepheids, Bumpers, Supernovae, novae, eclipsing variables). They are sampled with MACHO sampling and random Gaussian noise is added. All networks are trained using the Netlab package¹⁴. The output of the network is the posterior probability of microlensing.

Figure 1 shows the locations of ≈ 22000 lightcurves. The data for the

red and blue passbands are processed separately with neural networks to give outputs y_R and y_B . The decision boundary is shown in the bold broken line – convincing microlensing candidates have $y_{R,B} > 0.84$. This boundary is fixed by insisting that the number of false negatives in the entire MACHO dataset is $\lesssim 1$. This corresponds to a false positive rate of 0.3%. The 29 candidate microlensing lightcurves identified by Alcock et al.⁹ are denoted by filled black dots, while all other lightcurves are shown as open grey dots. Twelve of these 29 lightcurves satisfy $y_{R,B} > 0.84$, namely 1a, 1b, 5, 6, 10a, 11, 14, 21-25. There are additionally 2 false positives. Both lie close to the noise/microlensing border in parameter space.

After successfully passing the first tier of neural networks, Belokurov et al.¹³ apply a second tier that discriminates against supernovae (SNe) occurring in background galaxies behind the LMC. The colours change dramatically during a supernova explosion as a result of complicated radiation processes inside the ejecta. After a fairly constant pre-maximum epoch with $B - V \approx 0$, a supernova of type Ia typically starts turning red at the time of the maximum light. It reaches $B - V \approx 1$ in about 30 days and then drops back¹⁵. This can be contrasted with the colour behaviour during gravitational microlensing. Gravity bends light irrespective of its frequency. Therefore, colour does not change during microlensing. However, the achromaticity of the lightcurve only holds good if the source star is resolved and the lens is dark. The presence of other stars within the centroid of light or lensing by a luminous object will result in a colour change during the event. At the baseline, the colour is defined by the combined flux from all the sources. The amplified star will contribute most of the colour around the peak. The colour of a microlensing event can become redder or bluer, depending on the population of the blend, but it usually changes symmetrically about the peak with substantial correlation between passbands¹⁶. The differing behaviour of colour evolution during SNe and blended microlensing can be quantified as features fed to neural networks, and – as Belokurov et al.¹³ show – used to distinguish between the two. This leads to the discarding of a further 3 of the 12 candidates that passed the first tier.

Based on a neural network analysis, Alcock et al.’s sample is seriously contaminated. There are 6 almost certain microlensing events (1, 5, 6, 14, 21 and 25) and two likely ones (9, and 18). Some of the lightcurves rejected by the neural networks, but classified as microlensing by Alcock et al., are shown in Figure 2. The peak of the alleged event is shown as a vertical dashed line. Notice that event 23 – which looks perfect and passes all the

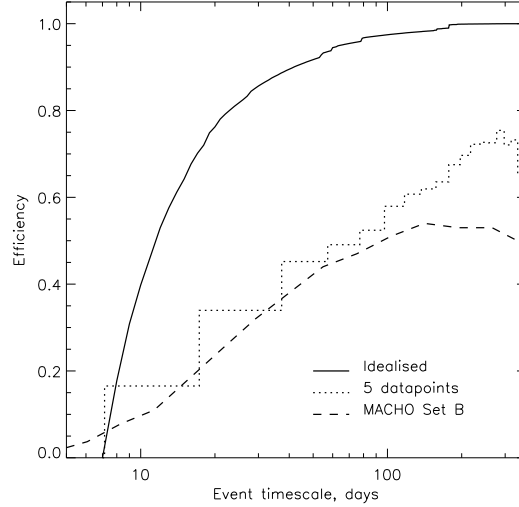


Figure 3. This shows three approximations to the efficiency as a function of Einstein diameter crossing timescale t . The full curve is the idealised efficiency calculated by integration over the distribution of sampling gaps. This is an upper limit. The dashed curve is the published efficiency of Alcock et al. (2000). This is a lower limit. The histogram is a realisation of the true efficiency derived from Monte Carlo simulations of event selection in the training set.

neural networks – has been shown by the EROS collaboration¹⁷ to have a second peak on the lightcurve about 7 years after the first one probed by MACHO and so is an unusual variable star. This is very worrisome for all microlensing experiments.

3. The Optical Depth

The conventional formula for optical depth is

$$\tau = \frac{\pi}{4} \frac{1}{N_{\star} T} \sum_j \frac{t_j}{\epsilon(t_j)} \quad (1)$$

where t_j is the Einstein diameter crossing time of the j th event, ϵ is the efficiency, T is the duration of the experiment and N_{\star} is the number of stars monitored. The summation is taken over the set of microlensing events. There are three major components to the efficiency. The first arises from shortcomings in the cuts used to identify microlensing events. The second arises from blending, which causes both the magnification and the number of stars monitored to be underestimated. The third arises from

the temporal sampling, as events are necessarily missed if they fall in a gap in the data-taking. A neural network, properly trained, will all but eliminate any contribution from the first component for the subset of events included in the training set. The second component cancels out to lowest order, as the loss due to the underestimate of the magnification is balanced by the gain due to the fact that an object may contain more than one star¹⁸. The third component of the efficiency still remains, but fortunately is straightforward to compute.

Figure 3 shows upper and lower bounds to the efficiency as a function of timescale. An upper bound to the efficiency can be found by assuming that events are missed if and only if no data are taken during the bump. We sum the distribution of sampling gaps over the baseline of the experiment and judge an event to be missed if it falls within a gap. The probability of missing an event with timescale t is just

$$P(t) \propto \sum_{t' \geq t} t' n(t') \quad (2)$$

where $n(t)$ is the number of gaps of duration t . The quantity $1 - P(t)$ is an idealised efficiency which is shown as a full curve in Figure 3. A lower bound to the efficiency is given by the published efficiency results of Alcock et al.⁹ for the looser set of candidates. This is because the neural networks necessarily provide a cleaner set of microlensing candidates, uncontaminated by spurious events. A realisation of the actual efficiency is easily found from Monte Carlo simulations of the training set, by finding the fraction of all events that are included (and hence will be inexorably characterised as microlensing by the network). In the simulations, microlensing events are generated with uniform priors. Only those events with five or more datapoints with a signal-to-noise greater than 5 are incorporated into the training set. The efficiency is therefore the ratio of events accepted into the training set to all events. The result is shown as a histogram in Figure 3, and lies between the upper and lower bounds, as expected.

Applying eq. (1) to the set of 9 events found by the neural network, we obtain the following bound on the optical depth to the LMC:

$$3 \times 10^{-8} < \tau < 5 \times 10^{-8}. \quad (3)$$

Here, the timescales uncorrected for blending given in third column of Table 7 of Alcock et al.⁹ are used. This is correct, as the effects of blending cancel out to lowest order.

This is a low value for the optical depth. The optical depths of the thin disk, thick disk and spheroid to be 2.2×10^{-8} , whilst the optical depth

of the stellar content of the LMC to be 3.2×10^{-8} on average. In other words, *our total optical depth matches the contribution from the known stellar populations in the outer Galaxy and the LMC. This implies that there is no contribution needed from compact objects in the halo.*

There is supporting evidence for this belief from the exotic events and from the lensing signal towards the Small Magellanic Cloud (SMC). First, the exotic events yield additional information which can break some of the microlensing degeneracies and thus give indirect evidence on the location of the lens. All the exotic lenses belong to known stellar populations in the outer Milky Way or the LMC. Second, the duration of the events towards the SMC is very different from the duration towards the LMC. The EROS collaboration¹⁹ constrain the optical depth towards the SMC to be $< 10^{-7}$ at better than the 90 % confidence level, based on an admittedly small sample. Both these facts militate against the idea that a single population of objects in the Milky Way halo is causing the microlensing events

4. Conclusions

The MACHO Era is over! The dark matter in the halo of the Milky Way is **not** in the form of massive, compact halo objects. The microlensing signal detected by both the MACHO and EROS experiments is entirely consistent with that expected from stellar lenses in the known populations. In particular, the sample of 14 high quality microlensing events in Alcock et al.⁹ is contaminated. Realistically, Alcock et al.'s sample has 6 almost certain microlensing events (1, 5, 6, 14, 21 and 25) and two likely ones (9, and 18). This is consistent with expectations from known stellar populations.

Even for the die-hards, the matter will surely soon be settled by the POINT-AGAPE experiment²⁰. This is a microlensing experiment towards the nearby Andromeda galaxy (M31), which probes a new line of sight through the Milky Way and M31 dark haloes. It will provide a new estimate of the fraction of the Milky Way and M31 dark haloes that is composed of MACHOs. Two fields north and south of the M31 bulge have been monitored for three years using the Wide Field Camera on the Isaac Newton Telescope. The POINT-AGAPE collaboration have already found a small number of interesting individual microlensing events towards M31²⁰, carried out a survey for classical novae²¹ and reported the locations, periods and brightness of ~ 35000 variable stars²². Very recently, an unrestricted and fully automated search for microlensing events towards M31 has been published²³. Using a series of seven cuts based on sampling, goodness of

fit, consistency, achromaticity, position in the colour-magnitude diagram and signal-to-noise. This leaves just 3 first-level or convincing microlensing candidates and 3 second-level or possible microlensing candidates. The efficiency of this survey is being computed at the moment and will yield an independent estimate of the MACHO fraction.

Die-hards have only a short time to wait.

References

1. F. Zwicky, *Morphological Astronomy*, Springer-Verlag, Berlin (1957)
2. M.S. Roberts, A.H. Rots, *A&A* **26**, 483 (1974); M.S. Roberts, R.N. Whitehurst, *ApJ* **201**, 327 (1975)
3. J.P. Ostriker, P.J.E. Peebles, A. Yahil, *ApJ* **193**, L1 (1974)
4. K. Griest, *ApJ* **366**, 412 (1991)
5. M.J. Rees, In *IAU Symposium 127: Dark Matter in the Universe*, eds. J. Kormendy, G.R. Knapp, Reidel, Dordrecht, p. 396
6. J.E. Gunn, In *IAU Symposium 127: Dark Matter in the Universe*, eds. J. Kormendy, G.R. Knapp, Reidel, Dordrecht, p. 543
7. D. Lynden-Bell, In *IAU Symposium 127: Dark Matter in the Universe*, eds. J. Kormendy, G.R. Knapp, Reidel, Dordrecht, p. 530
8. B. Paczyński, *ApJ* **304**, 1 (1986)
9. C. Alcock et al., *ApJ* **542**, 281 (2000)
10. T. Lasserre et al., *A&A* **355**, L39 (2000)
11. K. Sahu, *Nature* **370**, 275 (1994); N.W. Evans, G. Gyuk, M.S. Turner, J.J. Binney, *ApJ* **501**, L45 (1998); H.S. Zhao, *MNRAS* **294**, 139 (1998); H.S. Zhao, N.W. Evans, *ApJ* **545**, L35 (2000)
12. C. Alcock et al., *ApJ* **479**, 119 (1997)
13. V. Belokurov, N.W. Evans, Y. Le Du, *MNRAS* **352**, 233 (2004)
14. I.T. Nabney, *Netlab*, Springer-Verlag, New York (2002)
15. M.M Phillips, P. Lira, N.B. Suntzef, R.A. Schommer, M. Hamuy, J. Maza, *AJ* **118**, 1766 (1999)
16. R. Di Stefano, A.A. Esin, *ApJ* **448**, L1 (1995)
17. J.F. Glicenstein, Talk at the Hawaiian Gravitational Microlensing Workshop, 2004
18. C. Afonso et al., *A&A* **400**, 951 (2003)
19. C. Afonso et al., *A&A* **404**, 145 (2003)
20. S. Paulin-Henriksson et al., *A&A* **405**, 15 (2003); S. Paulin-Henriksson et al., *ApJ* **576**, L121 (2002); J. An et al., *ApJ* **601**, 845 (2004)
21. M. Darnley et al., *MNRAS* **353**, 571 (2004)
22. J. An et al., *MNRAS* **351**, 1071 (2004)
23. V. Belokurov et al., *MNRAS*, in press (astro-ph/0411186)